Kinesin-3 and dynein cooperate in long-range retrograde endosome motility along a nonuniform microtubule array

Martin Schuster[a], Sreedhar Kilaru[a], Gero Fink[b], Jérôme Collemare[c,*], Yvonne Roger[a], and Gero Steinberg[a]

[a]Department of Biosciences, University of Exeter, Exeter EX4 4QD, United Kingdom; [b]Max Planck Institute of Molecular Cell Biology and Genetics, D-01307 Dresden, Germany; [c]Laboratory of Phytopathology, Wageningen University, 6708 PB Wageningen, The Netherlands

ABSTRACT **The polarity of microtubules (MTs) determines the motors for intracellular motility, with kinesins moving to plus ends and dynein to minus ends. In elongated cells of *Ustilago maydis*, dynein is thought to move early endosomes (EEs) toward the septum (retrograde), whereas kinesin-3 transports them to the growing cell tip (anterograde). Occasionally, EEs run up to 90 µm in one direction. The underlying MT array consists of unipolar MTs at both cell ends and antipolar bundles in the middle region of the cell. Cytoplasmic MT-organizing centers, labeled with a γ-tubulin ring complex protein, are distributed along the antipolar MTs but are absent from the unipolar regions. Dynein colocalizes with EEs for 10–20 µm after they have left the cell tip. Inactivation of temperature-sensitive dynein abolishes EE motility within the unipolar MT array, whereas long-range motility is not impaired. In contrast, kinesin-3 is continuously present, and its inactivation stops long-range EE motility. This indicates that both motors participate in EE motility, with dynein transporting the organelles through the unipolar MT array near the cell ends, and kinesin-3 taking over at the beginning of the medial antipolar MT array. The cooperation of both motors mediates EE movements over the length of the entire cell.**

Monitoring Editor
Fred Chang
Columbia University

Received: Mar 14, 2011
Revised: Jul 22, 2011
Accepted: Jul 29, 2011

INTRODUCTION

Long-range organelle transport organizes eukaryotic cells and enables communication over large distances (Gross, 2004, Welte, 2004). The importance of long-range motility is illustrated by the fact that numerous neuronal diseases are related to defects in axonal transport (Chevalier-Larsen and Holzbaur, 2006; Duncan and Goldstein, 2006). Long-range intracellular membrane trafficking utilizes microtubules (MTs) and is driven by the molecular motors kinesin and dynein (Vale, 2003; Hirokawa and Takemura, 2004). MTs are tubulin polymers that expose β-tubulin at their more dynamic plus end (Nogales *et al.*, 1999). Motors recognize this intrinsic polarity, with kinesins generally moving to the plus ends and dynein traveling to the minus ends (Vale, 2003). Kinesin and dynein motor systems often oppose each other, thereby mediating bidirectional organelle transport (Gross *et al.*, 2002a; Müller *et al.*, 2008; Ally *et al.*, 2009; Hendricks *et al.*, 2010). In most cell types, the motors counteract one another while being bound to the same organelle. They seem to coordinate their activity in a tug-of-war (Müller *et al.*, 2008; Soppina *et al.*, 2009; Hendricks *et al.*, 2010), often in conjunction with higher-order control by regulatory factors (Welte *et al.*, 1998, 2005; Gross *et al.*, 2002a; Deacon *et al.*, 2003, 2005; Larsen *et al.*, 2008). This leads to bidirectional cargo motion, with individual runs normally spanning a few micrometers (Welte *et al.*, 1998; Shubeita *et al.*, 2008; Soppina *et al.*, 2009).

In elongated animal neurons, organelle transport is very persistent, with individual runs extending over 35 µm and more (Lee *et al.*,

This article was published online ahead of print in MBoC in Press (http://www.molbiolcell.org/cgi/doi/10.1091/E11-03-0217) on August 10, 2011.

*Present address: Laboratory of Phytopathology, Wageningen University, 6708 PB Wageningen, The Netherlands.

Author contributions: MS performed experiments, generated strains, and analyzed data; SK generated the temperature-sensitive Kin3^{ts} and the Grc1-GFP$_3$ strains; GF generated strains and analyzed the degree of MT bundling; JC generated strain AB33ΔKin3_Kin3G_ChRab5a and analyzed colocalization of EEs and kinesin-3; YR generated strain AB33ΔKin3_rDyn1_GRab5a and analyzed the localization of dynein and endosomes and the run length of EEs in Kin3^{ts} mutants; and GS conceived the project, analyzed data, and wrote the manuscript.

Address correspondence to: Gero Steinberg (G.Steinberg@exeter.ac.uk).

Abbreviations used: CM, complete medium; EE, early endosome; GFP, green fluorescent protein; mRFP, monomeric red fluorescent protein; MT, microtubule; MTOC, microtubule-organizing center; NM, nitrate-minimal medium; ORF, open reading frame; YFP, yellow fluorescent protein.

2003; Smith *et al.*, 2004; Barkus *et al.*, 2008). Such long-range forward motion is mediated by kinesin-3 (Barkus *et al.*, 2008), and kinesin-3 localizes to dynein-driven organelles (Koushika *et al.*, 2004) and travels in a bidirectional manner (Zhou *et al.*, 2001; Lee *et al.*, 2003; Barkus *et al.*, 2008). Interestingly, mutations in kinesin-3 inhibit both anterograde and retrograde organelle motility in *Drosophila melanogaster* (Barkus *et al.*, 2008). It is not known how defects in kinesin-3 affect retrograde membrane trafficking. One possibility is that kinesin-3 and dynein bind to the same organelle with the presence of kinesin-3 activity being required for dynein-based motility. Such a scenario was recently described for peroxisomal movements (Ally *et al.*, 2009). Another option is that kinesin-3 has a more active role in retrograde motility. This, however, would require a bipolar MT orientation, with plus ends directed to both ends of the cell. Neuronal dendrites contain such antipolar MTs (Baas *et al.*, 1988; Baas, 1999), which indeed allow the dynein motor to support anterograde and retrograde dendritic transport (Kapitein *et al.*, 2010).

In this study, we used the fungus *Ustilago maydis* to investigate the role of kinesin-3 in early endosome (EE) motility. This fungus is a genetically tractable model system with high similarity to mammalian neurons (Steinberg and Perez-Martin, 2008). Its elongated hyphal cells are ~80–100 μm long and grow at the cell tip, forming a septum at the rear cell end. EEs move processively toward the hyphal tip (anterograde) and backward toward the septum (retrograde). The biological function of this transport is not known, but it has been speculated that retrograde EE motility mediates communication between the hyphal tip and the nucleus (Steinberg, 2007), which is positioned in the middle of the cell. The elongated hyphal cells of *U. maydis* contain long MTs (Steinberg *et al.*, 2001) that form an antipolar MT array, with plus ends being directed to both cell poles (Lenz *et al.*, 2006). Long-range EE motility in fungi occurs along MTs (Wedlich-Söldner *et al.*, 2000) and, as in animals, is mediated by the motors dynein and kinesin-3 (Wedlich-Söldner *et al.*, 2002a). In elongated hyphal cells, it was shown that kinesin-3 supports anterograde motility of EEs, whereas retrograde motility is thought to be mediated by cytoplasmic dynein (Lenz *et al.*, 2006). Kinesin-3 is permanently bound to the EEs, whereas dynein only transiently binds to the organelles. Dynein binding and unbinding is thought to be a stochastic process that reverses the transport direction from anterograde to retrograde and vice versa (Schuster *et al.*, 2011a). Surprisingly, kinesin-3 was found on both anterograde and retrograde EEs, suggesting that it is a passive cargo on organelles moving in a retrograde direction (Schuster *et al.*, 2011a). In this paper, we show kinesin-3 has an active role in the motility of EEs and is the major motor for retrograde motility. By taking over from dynein at the barrier between unipolar MT and antipolar MT bundles, kinesin-3 supports long-range motility of EEs.

RESULTS

Hyphal cells contain an extended antipolar array of MT bundles

Under laboratory conditions, the fungus *U. maydis* forms elongated hyphal cells that expand at the growing cell tip and form septa at the proximal cell pole (Figure 1A). Using the plus end–binding EB1 homologue Peb1 fused to the yellow fluorescent protein (Peb1-YFP; Straube *et al.*, 2003), researchers previously reported that MTs form a unipolar MT array near the cell tip (Schuchardt *et al.*, 2005), but form an antipolar array in the middle region of the cell (Lenz *et al.*, 2006). We performed a more detailed study using Pep1-YFP, and found that >96% of the MT plus ends elongate toward both cell poles, suggesting they form regions of unipolar MT orientation at both cell ends (Figure 1, B and C; Supplemental Movie S1). In the middle part of the cell, MTs grew toward both cell poles, indicating that MTs have an antipolar orientation (Figure 1C). To gain further insight into the organization of the MT array, we established a putative γ-tubulin ring complex protein (Grc1, RefSeq accession number: XP_757621.1) as a marker for cytoplasmic MT-organizing centers (MTOCs). Grc1 is 22.9% identical with Alp4 from fission yeast and 22.5% identical with human GCP-2, and shares with them a Spc97_Spc98 domain (Figure 1D; p values are given). We fused a triple-tag of the green fluorescent protein (GFP) to the C-terminus of the endogenous *grc1* gene and expressed it under its native promoter. Consistent with its assumed role in MT nucleation, Grc1-GFP_3 localized at the pole of mitotic spindles (Figure 1E). In hyphal cells, Grc1-GFP_3 was mainly found at the spindle pole (Figure 1F). In addition, distinct Grc1-GFP_3 spots were scattered around the middle region of the cell (Figure 1, F and G). The signals were not motile (Movie S2) and were located at the ends of cytoplasmic MTs within a bundle (Figure 1H), as indicated by the increase of mCherry-Tub1 fluorescence intensity (Figure 1I). This suggests that the signals label MT minus ends at cytoplasmic MTOCs. Almost no Grc1-GFP_3 signals were located within the 10–15 μm behind the hyphal tip (Figure 1K) and the septum (Supplemental Figure S1). This is consistent with a unipolar orientation of MTs at both cell ends.

We visualized MTs by expressing GFP fused to α-tubulin (GFP-Tub1; Steinberg *et al.*, 2001), and found that cells contained on average approximately two continuous MT tracks (Figure S2A). The fluorescence intensity of these tracks was stronger in the cell center than toward the cell poles (Figure 2A, compare cross-sections 1 and 4; three-dimensional reconstruction from *z*-axis stacks; Movie S3). Such an increase in intensity reflects a higher number of MTs in a bundle (Straube *et al.*, 2006), suggesting MTs have a strong tendency to form bundles in this part of the hyphal cell. Indeed, MTs of weaker intensity disappeared when depolymerizing, suggesting they are unbundled tubulin polymers (unpublished data). We measured the signal intensity in MT tracks and compared it to the signal intensity of single and unbundled MTs. From this, we estimated that most tracks consist of two to four MTs, which is in the range of MT bundling in yeast-like cells of *U. maydis* (Straube *et al.*, 2006). Single MTs were mainly found near the cell ends, whereas almost all MTs were bundled in the central cell region (Figure 2B; only one-half of the cell is shown). To see whether these MT bundles contain uni- or antipolar-oriented MTs, we coexpressed the plus end–binding protein Peb1 fused to monomeric red fluorescent protein (mRFP) and GFP-Tub1. In bundles within the central part of the cell, Peb1-mRFP signals moved away from each other (Figure 2C), demonstrating they are antipolar, whereas unipolar MT bundles were found near the cell poles (Figure 2D). Taken together, these data show that hyphal cells contain an MT array consisting of unipolar MTs at the cell poles and antipolar bundles throughout the cell center.

EEs travel across the entire MT array

In *U. maydis* cells, EEs move rapidly in a bidirectional manner (Wedlich-Söldner *et al.*, 2000). Their large number, however, makes it very difficult to follow individual organelles over longer distances. To avoid interferences between EEs, we visualized single organelles by expressing a fusion protein of photoactivatable GFP fused to the endosomal GTPase Rab5a (Schuster *et al.*, 2011b). When this marker was activated by a 405-nm laser pulse at the hyphal tip (Figure 3A, arrowhead), we occasionally observed single EEs that continuously moved in retrograde direction (Figure 3A and Movie S4). After activation near the septum, many anterograde EEs processively moved toward the hyphal tip (Figure 3B), with the majority turning their transport direction within 50 μm of

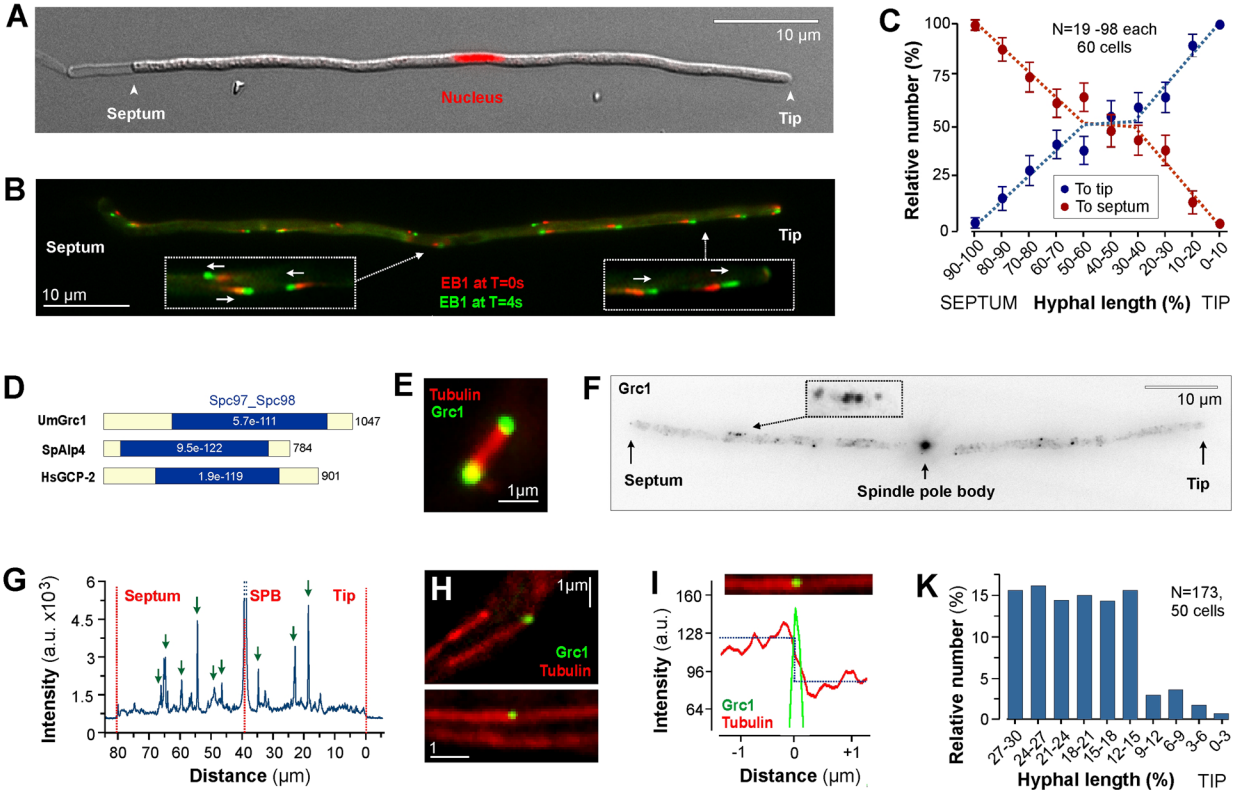

FIGURE 1: MT organization in hyphal cells of *U. maydis*. (A) A hyphal cell of *U. maydis*. The elongated cell extends at the growing tip and forms a septum at the opposite cell end. The nucleus is positioned close to the cell middle. (B) Overlay of two images taken at 4-s time interval showing Peb1-YFP motility in a hyphal cell. Insets show antipolar MT orientation in the cell middle and unipolar MT orientation near the cell tip. See also Movie S1. (C) Graph indicating the orientation of Peb1-YFP motility in hyphal cells. Peb1 is a homologue of EB1 and was used to label growing MT plus ends (Straube *et al.*, 2003). Sample size (N) for Peb1-YFP signals and cell number are given. (D) Domain organization of γ-tubulin ring complex proteins in *U. maydis* (UmGrc1), *Schizosaccharomyces pombe* (SpAlp4), and humans (HsGCP-2). Note that all putative proteins contain a highly conserved Spc97_Spc98 domain (p values give in white numbers). (E) Colocalization of Grc1-GFP$_3$ and mCherry-α-tubulin in a mitotic cell. The γ-tubulin ring complex protein concentrates at the spindle poles, confirming that it is part of the MTOCs. (F) Distribution of Grc1-GFP$_3$-labeled MTOCs in a hyphal cell. Most Grc1-GFP$_3$ concentrates at the spindle pole body. Additional signals are scattered along the central region of the cell (inset), indicating the presence of cytoplasmic MTOCs. Image was contrast-inverted. See also Movie S2. (G) Graph showing a signal-intensity profile over a hyphal cell. Peaks of higher intensity most likely indicate MTOCs at MT minus ends (green arrows). Note the absence of peaks near the septum and the tip of the cell. (H) Colocalization of Grc1-GFP$_3$ and mCherry-labeled MTs in the apical region of a hyphal cell. (I) Graph showing a signal-intensity profile over an MT bundle. The Grc1-GFP$_3$ signal peak is located at a stepwise increase in mCherry-Tub1 signal intensity, suggesting that it marks an MTOC in an MT bundle. (K) Bar chart showing the distribution of Grc1-GFP$_3$-labeled MTOCs relative to the hyphal tip. Almost no MTOCs are located within the apical 10–12 µm. Sample size (N) for cytoplasmic Grc1-GFP$_3$ signals and cell number are given.

travel (Figure 3B). However, some EEs traveled over longer distances and reached into the region of unipolar MT orientation at the rear cell pole, where the septum is formed (Figure 3, A and B, and Movie S4), suggesting they switch from minus end– to plus end–directed motility within the antipolar MT array. Interestingly, retrograde organelles often paused shortly after they left the tip (Figure 3, A, inset, and C). These pauses lasted for 0.2–0.3 s (Figure 3D), and usually occurred ~10–20 µm behind the cell tip, which coincided with entry into the antipolar MT region (Figure 1, C and K). To test whether this zone represented a transition into the antipolar MT region, we coimaged Grc1-GFP$_3$ and photoactivatable mCherry (Subach *et al.*, 2009) fused to Rab5a. We found that EEs often paused when reaching a Grc1-GFP$_3$ signal (Figures 3E and S3). This suggests that cytoplasmic nucleation sites pose obstacles for the retrograde organelles.

The similarity in the motility behavior of EEs coming from opposite poles and the symmetric organization of the MT array suggested the underlying transport mechanism might be similar in both directions. It was shown that retrograde EE motility involves dynein released from a comet-like accumulation at MT plus ends (Lenz *et al.*, 2006; Schuster *et al.*, 2011b). Consistent with the symmetry of the MT array, we found such dynein comets at MT plus ends at both poles of the cell (Figure 4A). From here, dynein leaves to travel toward the cell center (Figure 4B). Next, we inhibited EE motility in a temperature-sensitive dynein mutant. After 120 min at restrictive temperature (32°C; Figure 4C) EEs clustered at the plus ends near the tip and the septum, respectively; it has been suggested this is due to the unbalanced activity of kinesin-3 (Lenz *et al.*, 2006). However, significantly fewer EEs concentrated near the septum ($p = 0.0334$; Figure 4D), suggesting that fewer EEs travel to the

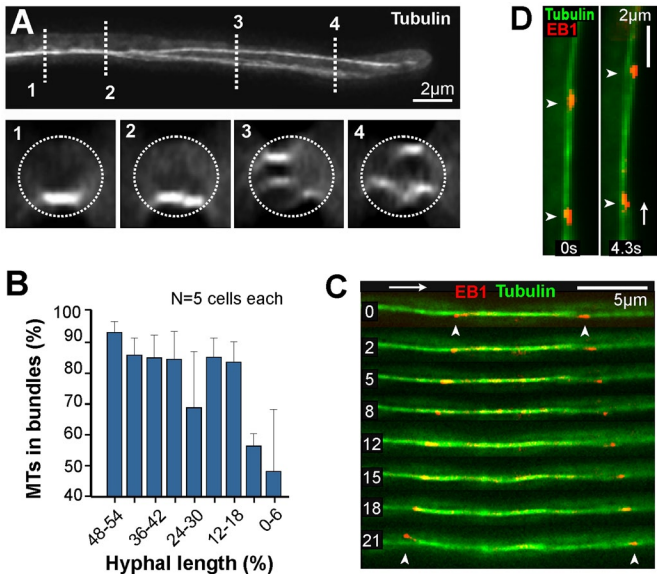

FIGURE 2: Bundling of MTs. (A) Maximum projection of a *z*-axis stack of GFP-Tub1-labeled MTs. Near the hyphal tip ~50% of all MTs are gathered in brighter MT bundles (cross-section 3 and 4). The degree of bundling increases toward the middle region of the cell (cross-section 1 and 2). See also Movie S3. (B) Degree of bundling estimated from quantitative fluorescence microscopy on GFP-α-tubulin MTs. This method was previously validated by electron microscopy studies (Straube *et al.*, 2006). Sample size (N) for MT bundling in separate cells and total number of analyzed signals are given. (C) Peb1-RFP-labeled plus ends within a bipolar MT bundle located in the central part of the hyphal cell. The motility of the EB1 homologue indicates that the bundle consists of antipolar-oriented MTs. Time is indicated in seconds. The location of the cell tip is indicated by an arrow. (D) Peb1-RFP-labeled plus ends within an MT bundle located in the apical part of the hyphal cell. The motility of the EB1 homologue indicates that the bundle consists of unipolar-oriented MTs. Time is indicated in seconds. The location of the cell tip is indicated by an arrow.

septum than to the tip. We tested this by measuring EE flux at 5 µm behind the tip and the septum, and found significantly less EE motility at the rear cell end ($p < 0.0001$; Figure 4E). This difference is most likely due to a slight asymmetry in the MT array, as an increased number of Peb1-YFP comets were found at the hyphal tip rather than near the septum (Figure 4F), indicating that more MTs were growing toward the hyphal tip than toward the septum. Thus the MT array is slightly asymmetric, which causes a bias for EE motility toward the growing cell tip.

Dynein supports short-range retrograde EE motility

In *U. maydis*, cytoplasmic dynein supports minus end–directed EE transport (Wedlich-Söldner *et al.*, 2002a; Lenz *et al.*, 2006), and it is able to travel over long distances (Schuster *et al.*, 2011a). To investigate whether dynein plays a role in EE long-range retrograde transport, we observed GFP-Rab5a in mutants containing a temperature-sensitive dynein allele (*dyn2*^{ts}; Wedlich-Söldner *et al.*, 2002b). This allowed the observation of EE motility in the absence of functional dynein before a steady-state situation was reached, a point at which the organelles became trapped at plus ends due to the unbalanced activity of kinesin-3 (Lenz *et al.*, 2006). At permissive temperature (22°C), EEs showed bidirectional motility (Figure S4). When hyphal cells were shifted to restrictive conditions for 30 min, EEs started to accumulate at plus ends near the hyphal tip (asterisk in Figure 5, A and B). No retrograde motility was found in ~10 µm of the apical region (average: 9.63 ± 2.88; n = 30; Figure 5, A and B, and Movie S5), suggesting dynein is not functional and therefore cannot overcome the unipolar MT array near the cell ends. The lack of motility was not due to changes in MT track numbers or a change in their orientation at 32°C (Figure S2, A and B). However, those EEs that had not yet become trapped at plus ends still traveled over long distances in the central part of the cell (Figure 5A, arrowheads), and their run length was even slightly enhanced in the dynein mutant (Figure 5C; different from control; Mann-Whitney test, $p = 0.013$). These results suggest dynein is crucial for short-range retrograde motility within the unipolar MT array near the hyphal tip, whereas subapical long-range EE motility does not require dynein. We also noted that the inactivation of dynein increased the length of the MTs (Figure 5D), a phenomenon previously described (Adamikova *et al.*, 2004). We expressed Peb1-YFP in temperature-sensitive dynein mutants and found inactivation of dynein increased the fluorescence intensity of Peb1-YFP, suggesting more of the EB1 homologue binds to MT plus ends in the absence of dynein (Figure 5, E and F). Fungal EB1 fosters MT assembly (Blake-Hodek *et al.*, 2010), suggesting the increase in Peb1 causes the elongation of the MTs in dynein mutants.

To understand the role of dynein in long-range motility in subapical regions, we simultaneously observed mCherry-Rab5a and GFP_3Dyn2. In agreement with the proposed role of dynein in the distal part of the hyphal cell, we found a high degree of colocalization in the first 10 µm (Figure 6A). In more subapical regions, however, an increasing number of dynein signals lost their colocalizing with EEs (Figure 6A and Movie S6). Binding and unbinding of dynein to EEs in the apical region of the cell was reported to change the transport direction (Schuster *et al.*, 2011a). We found such cases also in the subapical parts of the hyphal cell (Figure 6B; filled arrowheads indicate dynein, open arrowheads the EE; spatial position relative to the cell apex is indicated in lower left corner of the kymograph; the position of the hyphal tip is indicated by an arrow). However, we also observed that organelles stopped moving (Movie S7) or continued traveling in retrograde direction after unbinding from dynein (Figures 6C–E and S5 and Movie S8). Taken together, these results suggest dynein supports motility along the unipolar parts of the MT array near the cell poles, whereas another motor supports retrograde motility within the antipolar array.

Kinesin-3 is required for long-range retrograde endosome transport

In yeast-like cells of *U. maydis*, EEs are transported solely by kinesin-3 and dynein (Wedlich-Söldner *et al.*, 2002a). To confirm that kinesin-3 and dynein are the only motors driving EE transport in the elongated hyphal cells, we replaced the promoter of dynein by the conditional *crg* promoter (Bottin *et al.*, 1996) in a kinesin-3 null mutant. When dynein was depleted in these mutant cells, EEs often clustered and almost no EE motility was seen (Figure 7A and Movie S9). This strongly indicates that EE motility in hyphal cells is mediated solely by kinesin-3 and dynein. As a consequence, we considered it likely that the retrograde EE motility in dynein mutants is mediated by kinesin-3. Indeed, kinesin-3 colocalized with retrograde EEs in all parts of the hyphal cell (Figure 7, B and C) and traveled over long distances in a retrograde direction (Movie S10).

To test whether kinesin-3 has an active role in retrograde EE motility, we investigated the effect of interference with kinesin-3 activity on EE motility. Existing conditional or deletion mutants did not form proper hyphae (Lenz *et al.*, 2006) and, consequently, did not allow investigation of long-range transport of EEs. We therefore generated

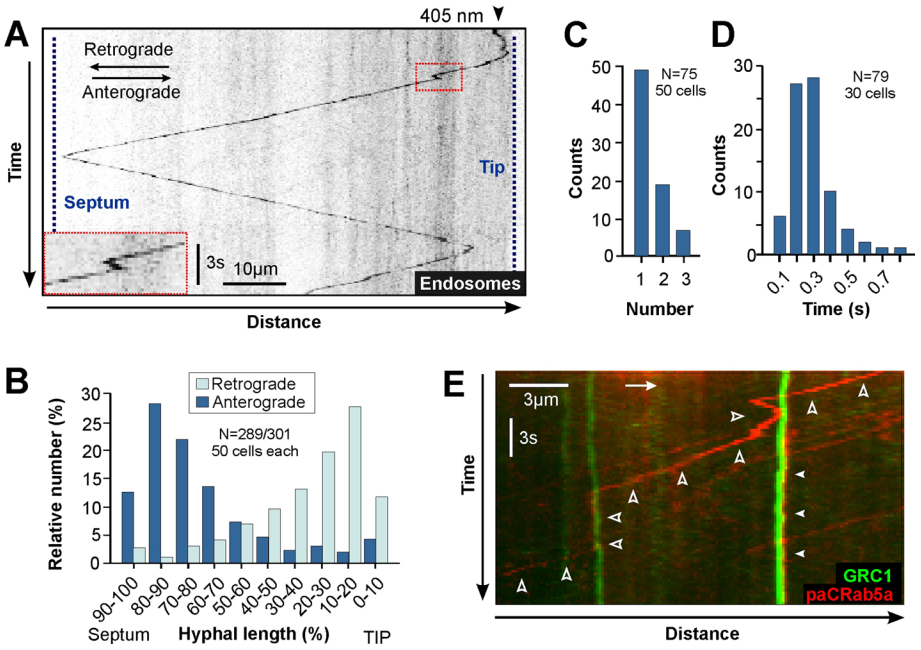

FIGURE 3: Motility of EEs labeled with photoactivatable GFP-Rab5a. (A) Kymograph showing motility of an EE moving in the retrograde direction, visualized after photoactivation of GFP-Rab5a with a 405-nm laser pulse at the hyphal tip (405 nm). The organelle travels continuously toward the septum (retrograde), where it turns and travels back toward the hyphal tip (anterograde). The inset shows an inconsistency in the trajectory of the organelle moving in the retrograde direction. See also Movie S4. (B) Run length of EEs photoactivated at the hyphal tip (light blue) or at the septum (dark blue) of hyphal cells. Sample size (N) for moving EEs and total number of analyzed cells are given. (C) Bar chart showing the number of pauses in retrograde EE trajectories. Sample size (N) for the number of retrograde moving EEs and total number of analyzed cells are given. (D) Bar chart showing the time that retrograde EEs stay in pause. Sample size (N) for the number of pausing events and total number of analyzed cells are given. (E) Kymograph showing colocalization of EEs moving in the retrograde direction (red, photoactivated mCherry fused to Rab5a) and cytoplasmic MTOCs (green, γ-tubulin ring complex protein Grc1-GFP$_3$). The location of the cell tip is indicated by an arrow. See Figure S3 for more examples.

a "fast-reacting" temperature-sensitive kinesin-3 allele (*kin3*^{ts}) in which kinesin-3 activity was abolished after shifting proper hyphal cells for a few minutes to restrictive temperature (see *Materials and Methods* for details). At permissive temperature (22°C), *kin3*^{ts} mutant strain formed long hyphal cells and normal bidirectional motility of EEs was found (Figure 7D, 22°C). After 5 min at restrictive temperature, motility was severely impaired (Figure 7D, 32°C) and the run length of the EEs was reduced ($p < 0.0001$; Figure S6). Interestingly, EEs began to cluster at 10–15 µm behind the tip (average: 12.43 ± 3.25 µm; n = 25; Movie S11), which was in good agreement with the appearance of the MT minus ends (Figure 1K), supporting the notion that kinesin-3 takes over from dynein at the beginning of the antipolar MT bundles. In most cells, EEs did not travel over the middle region of the cell (Figure 7D, red arrow, 32°C; Movie S11). With longer time at restrictive conditions, their motility further decreased, and clusters of EEs were found in the middle region of the cell (Figure S7). Some motility was still present, which could have been residual activity of Kin3^{ts} or due to dynein binding and subsequently moving stationary EEs.

In *Drosophila* cells, motor activity of kinesin is required to enable dynein-based motility (Ally *et al.*, 2009). This raised the possibility that the defect in EE motility is due to impaired dynein activity in the Kin3^{ts} mutants. To test this, we visualized Kin3^{ts}-GFP motor on EEs at restrictive and permissive temperatures. At permissive temperature, Kin3^{ts}-GFP and mCherry-Rab5a colocalized (Figure 8A). At restrictive temperature, the inactivated motor remained bound to the organelles (Figure 8B and Movie S11), suggesting that the temperature-sensitive mutations did not affect the attachment to the EEs, but rather impaired the motor activity of Kin3^{ts}. To see whether the inactive motor inhibits dynein activity, we analyzed the motility of dynein labeled with triple-GFP fused to its endogenous heavy chain (Schuster *et al.*, 2011b) in *kin3*^{ts} mutants. We found that dynein was able to leave the plus ends in cells where Kin3^{ts} was inactivated (Figure 8C), which confirmed previous findings that dynein leaves the plus end of MTs in *Kin3*^{rigor} mutants (Schuster *et al.*, 2011b). The velocity of this "free dynein" was not different from the velocity of retrograde dynein-bound EEs that traveled through the unipolar regions of the MT array after inactivation of the Kin3^{ts} (Figure 8D). Furthermore, the velocity of EEs was not impaired in *Kin3*^{ts} or *Dyn2*^{ts} mutants (Figure S8). Taken together, these results suggest 1) dynein and kinesin-3 do not influence each other's activity and 2) dynein takes EEs through the unipolar part of the MT array, whereas 3) kinesin-3 is the main motor for long-range EE motility across the antipolar MT array.

DISCUSSION

The organization and orientation of the MT array determine the use of motor proteins in membrane trafficking. In neurons, the axonal MT array is uniform, with the plus ends facing toward the growth cone (Burton and Paige, 1981; Heidemann *et al.*, 1981). Consequently, retrograde transport of EEs is based on the minus end–directed motor dynein (Ha *et al.*, 2008), which moves its cargo from the expanding growth cone back to the cell center (Vale, 2003; Hirokawa and Takemura, 2004). In contrast, dendrites contain a nonuniform MT array with unipolar regions at the tip of the dendrite and antipolar MT orientation within most parts of the elongated dendrite (Baas *et al.*, 1988, 1991). We show here that the MT organization in hyphal *U. maydis* cells corresponds with that in dendrites. Like dendrites, hyphal cells show a region of unipolar MT orientation at the cell poles, which is followed by antipolar MT bundles in the subapical region. This introduces *U. maydis* as a model system for long-range transport in dendrites. Our results demonstrate that kinesin-3 is supporting long-range motility of EEs along the antipolar MT bundles. It was reported that kinesin-3 localizes to dynein-driven organelles (Koushika *et al.*, 2004) and travels over long distances in a bidirectional manner (Zhou *et al.*, 2001; Lee *et al.*, 2003; Barkus *et al.*, 2008) in animal cells. We therefore consider it likely kinesin-3 plays similar roles in bidirectional organelle trafficking and is conserved from fungi to animal cells.

It is thought that the differences in neuronal MT organization are responsible for neuronal polarity and the structural differences between axons and dendrites (Baas *et al.*, 1988; Black and Baas, 1989; Baas and Lin, 2010). This is done by selective recruitment of motors, which allows dynein to transport Golgi membranes into dendrites, but not axons (Zheng *et al.*, 2008; Baas and Lin, 2010). In dendrites,

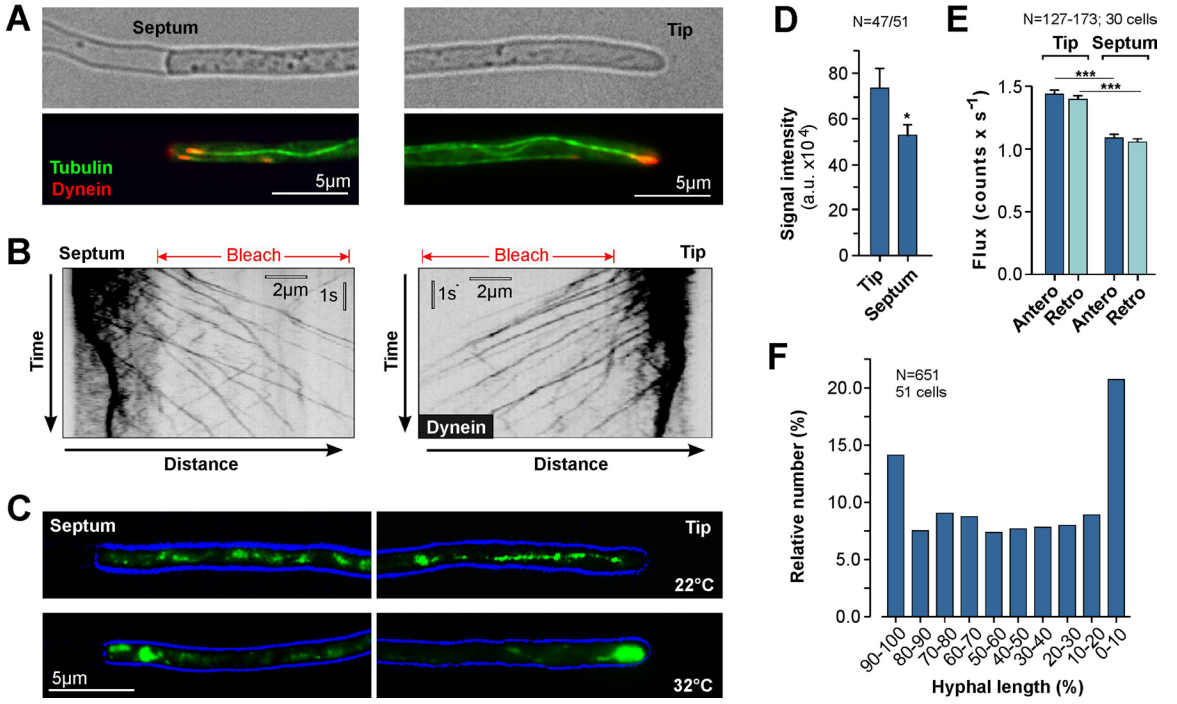

FIGURE 4: Dynein accumulations at MT ends near the tip and the septum. (A) GFP_3Dyn forms comets at MT ends (GFP-Tub1) near the septum and the growing tip. Note that dynein comets are regions of efficient EE capturing and are therefore considered a "loading zone," where arriving EEs bind to dynein for retrograde transport (Lenz *et al.*, 2006; Schuster *et al.*, 2011b). (B) Kymographs showing GFP_3Dyn leaving the dynein comets near the septum and the hyphal tip. Cells were photobleached to reduce the interfering signal background. Images are contrast-inverted. (C) Distribution of EEs in temperature-sensitive dynein mutants at permissive (22°C) or restrictive (32°C) temperatures. Inactivation of dynein results in an accumulation of the organelles at plus ends near the hyphal tip (Tip) or near the septum (Septum). (D) Bar chart showing fluorescence intensity of GFP-Rab5a at the tip and the septum of temperature-sensitive dynein mutants at restrictive temperature. Significantly fewer signals concentrate near the septum (*$p = 0.0334$), indicating that fewer EEs travel toward the plus ends at the rear cell pole than toward the growing hyphal apex. Sample size (N) for the number of EEs accumulations is given. (E) Bar chart showing the frequency of EE transport toward the tip and the septum. Significantly more anterograde and retrograde EE transport was found near the hyphal tip (***$p < 0.0001$). Sample size (N) for EEs moving in the anterograde and retrograde directions and number of analyzed cells are given. (F) Bar chart showing the relative number of Peb1-YFP comets at MT plus ends along the hyphal cell. More plus ends are concentrated at the hyphal apex, suggesting that more MTs support tipward transport of EEs. Note that this asymmetry most likely underlies the observed differences in EE trafficking. Sample size (N) for the total number of analyzed Peb1-YFP signals and number of analyzed cells are given.

bidirectional motility of dynein also supports stable distribution of vesicles (Kapitein *et al.*, 2010) and a similar mechanism might account for the presence of ribosomes in the dendrite (Baas and Lin, 2010). In fungi, ribosomes are also concentrated at the growing tip (Howard and Aist, 1979; Howard, 1981). Similar to dendrites, Golgi membranes in *U. maydis* are distributed along the hyphal cell, with a gradient toward the hyphal tip (Wedlich-Söldner *et al.*, 2002b; Steinberg and Schuster, 2011). The mechanism of ribosome and Golgi positioning in *U. maydis* is not known. However, if the situation is similar to that in dendrites, the antipolar MT array could help dynein to position ribosomes and Golgi vesicles. Thus the need to distribute organelles by minus-end motors might have dictated the organization of the MT array.

In most systems, dynein and kinesin motors are found on the same organelle (Hirokawa *et al.*, 1990; Rogers *et al.*, 1997; Gross *et al.*, 2002b; Ligon *et al.*, 2004; Pedersen *et al.*, 2006), where they counteract each other in a tug-of-war (Müller *et al.*, 2008; Soppina *et al.*, 2009; Hendricks *et al.*, 2010) or control each other's activity by physical interaction or binding to a common regulator (Welte *et al.*, 1998, 2005; Deacon *et al.*, 2005; Guillaud *et al.*, 2008; Larsen *et al.*, 2008). In *U. maydis*, kinesin-3 is always bound to the EEs, whereas dynein only transiently binds to the organelles (Schuster *et al.*, 2011a). When dynein meets an anterograde EE, it can bind the organelle, which changes the transport direction from anterograde to retrograde. Unbinding of dynein allows kinesin-3 to take over, which in the distal unipolar MT array results in a switch to anterograde motility toward the plus end at the hyphal tip (Schuster *et al.*, 2011a). The results summarized here suggest that in the subapical region, where MTs form antipolar bundles, kinesin-3 interacts with MTs of opposite orientation, thereby maintaining the retrograde transport direction (Figure 9). Our results suggest this change from dynein to kinesin-3-dependent retrograde motility often happens at cytoplasmic MTOCs, which might provide obstacles that foster the release of dynein. This short pause reflects the time needed for rebinding of the several kinesin-3 motors on the organelle that mediate the continued processive motility toward the plus ends near the septum. The organization of the MTs in bundles probably supports this mechanism. In yeast-like cells of *U. maydis*, the individual MTs within a bundle are only ~10 nm apart from each other (Straube *et al.*, 2006). It therefore seems likely that the three to five kinesin-3

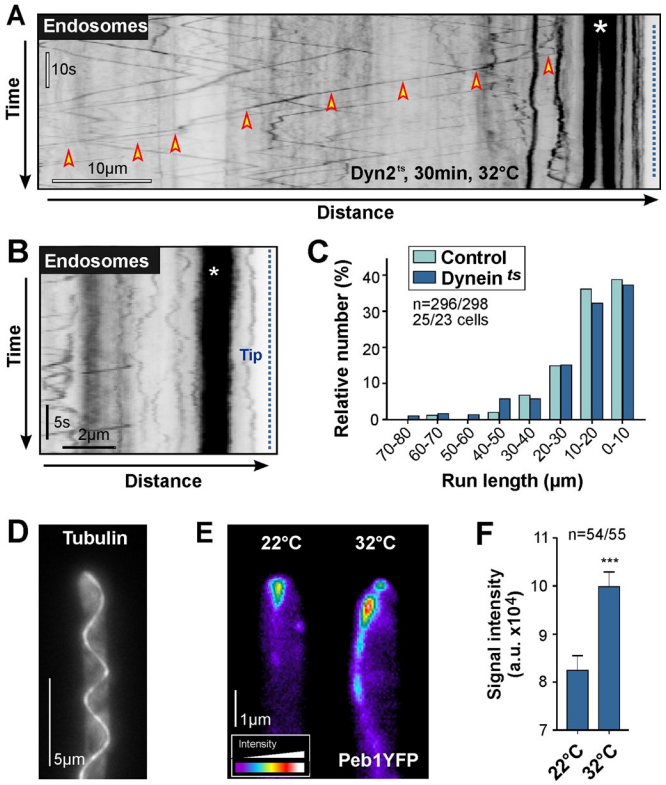

FIGURE 5: Retrograde motility of EEs in conditional dynein mutants. (A) Kymograph showing retrograde motility of EEs (GFP-Rab5a) in a temperature-sensitive dynein mutant at restrictive conditions. EEs accumulate within the region of unipolar MT orientation (*) but show long-range motility in the region of antipolar MTs (arrowheads). For control kymograph at 22°C, see Figure S4; see also Movie S5. (B) Kymograph showing EEs (GFP-Rab5a) in the apical region of a temperature-sensitive *dyn2*^{ts} hyphal cell. EEs cluster at plus ends near the hyphal cell tip (*). No motility is seen, indicating that dynein is inactivated. Note that MTs in this region have a unipolar orientation. The cell was shifted to 32°C for 30 min. (C) Bar chart showing retrograde run length of EEs in a *dyn2*^{ts} mutant cell at restrictive temperature. Note that no motility was seen in the first 10 µm in *dyn2*^{ts} mutants. To compare this subapical motility with control cells at restrictive temperature, the run length of EEs in control cells was measured starting 10 µm behind the tip. Sample size (N) for EEs moving in the retrograde direction and the total number of analyzed cells are given. (D) Images showing MTs (GFP-Tub1) in a Dyn2^{ts} mutant hyphal cell at restrictive temperature. In the absence of dynein, MTs become longer and often reach into the apex of the hyphal cell. The effect of dynein inactivation on MT length was reported previously (Adamikova *et al.*, 2004). (E) Pseudo-colored images of a fluorescent EB1 homologue (Peb1-YFP; Straube *et al.*, 2003) at apical plus ends in a temperature-sensitive dynein mutant. Note that more Peb1YFP is concentrated at MT tips at restrictive conditions (32°C). (F) Bar chart showing intensity measurements at apical plus ends in a temperature-sensitive dynein mutant at permissive (22°C) and restrictive conditions (32°C). Fungal EB1 was reported to enhance MT assembly (Blake-Hodek *et al.*, 2010), which might cause MT elongation in dynein mutants. Sample size (N) for analyzed Peb1-YFP signals at apical MT plus ends is given.

motors on a dynein-driven EE (Schuster *et al.*, 2011a) can bind to the adjacent MT within the bundle when the bipolar array begins. Unless this kinesin-3-driven EE meets a dynein that is released from the plus ends at the rear cell pole, it can continue moving toward the septum, where it finally reaches the end of the MT array. A dynein comet at the rear cell end ensures efficient loading onto dynein, keeping EEs from falling off the track (Schuster *et al.*, 2011b). Thus the symmetric organization of the MT array ensures bidirectional and long-range motility mainly based on the activity of kinesin-3.

An interesting question is why the switch between dynein and kinesin-3 occurs during retrograde EE motility. We show here that EEs move processively in retrograde and anterograde directions for up to 90 µm, from the hyphal tip all the way back to the septum. Similar long-distance motility of organelles was reported in other elongated cells (Koonce and Schliwa, 1986; Smith *et al.*, 2004; Miller *et al.*, 2005; Barkus *et al.*, 2008). While single motors are able to move an organelle (Shubeita *et al.*, 2008; Soppina *et al.*, 2009; Schuster *et al.*, 2011a), in vitro data indicate that single motors can only travel over one to a few micrometers (Howard *et al.*, 1989; Wang *et al.*, 1995; Thorn *et al.*, 2000; Reck-Peterson *et al.*, 2006). This is particularly well studied for dynein, which can move its cargo over ~1–2 µm (Wang *et al.*, 1995, King and Schroer, 2000; Mallik *et al.*, 2005), with a maximum run length of ~8–10 µm reported for dynein from *Saccharomyces cerevisiae* (Reck-Peterson *et al.*, 2006). We recently reported that single dynein motors in *U. maydis* move EEs (Schuster *et al.*, 2011a, 2011b). Thus dynein is most likely not able to transport EEs from the hyphal tip to the septum to the other cell end. However, when several motors of the same kind cooperate on the cargo, much larger distances can be traversed (Klumpp and Lipowsky, 2005; Mallik *et al.*, 2005; Vershinin *et al.*, 2007). We recently demonstrated that two to five kinesin-3 motors are bound to EEs in *U. maydis* and have modeled that four motors are sufficient to travel ~97 µm (Schuster *et al.*, 2011a). This is in agreement with our conclusion that the antipolar MT bundles allow kinesin-3 motors to move EEs over the large distances.

Why are EEs traveling over such long distances? In neurons, retrograde motility of EEs is involved in neurotrophic signaling between the distal synapsis and the cell body (Delcroix *et al.*, 2003; Miaczynska *et al.*, 2004; Howe and Mobley, 2005). By this mechanism, the nucleus receives information from the distal cell end. In *U. maydis*, the nucleus is positioned 40–50 µm behind the expanding tip and maintains this position while the cell expands. In an analogy to retrograde signaling in neurons, it has been speculated that retrograde EE motility supports communication between the cell tip and the nucleus (Steinberg, 2007). However, such a role for EEs does not explain the extended pole-to-pole runs by which EEs connect the tip and the septum. Long-range motility of EEs might serve another signaling aspect. When hyphal cells of *U. maydis* continuously expand at the growing tip, they simultaneously form septa at the rear cell end to move their cytoplasm forward (Steinberg *et al.*, 1998). This suggests that septum formation and tip advancement must be synchronized. We speculate that EEs provide the means to communicate between cell ends by random long-range walks along the antipolar MT array. While such a function of long-range motility of EEs in signaling is tempting, it must be emphasized that experimental evidence for such a role is currently missing.

Finding experimental evidence to support this proposed function is a fascinating challenge for the future.

MATERIALS AND METHODS

Strains and plasmids

The *U. maydis* strains AB33nRFP, AB33paGRab5a, AB33GT_Peb1R, AB33G$_3$Dyn2, and AB33G$_3$Dyn2_ChRab5a were described previously (Schuchardt *et al.*, 2005; Lenz *et al.*, 2006; Schuster *et al.*,

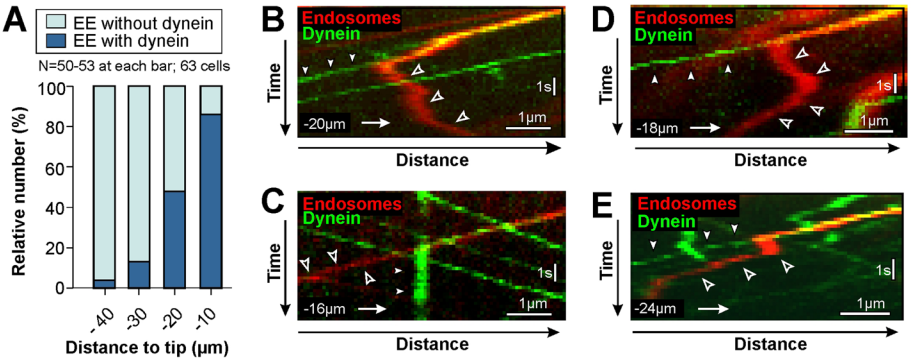

FIGURE 6: Colocalization of GFP_3Dyn and mCherry-Rab5a on retrograde EEs. (A) Bar chart showing the degree of colocalization of dynein and EEs. Sample size (N) for analyzed EEs moving in the retrograde direction and total number of analyzed cells are given. (B) Kymograph showing motility of mCherry-Rab5a on EEs (red) and motility of GFP_3Dyn (green). Dynein and the EE travel together until the EE reverses direction (open arrowheads), whereas dynein continues forward motility (filled arrowheads). The position relative to the tip is shown in the lower left corner. The location of the cell tip is indicated by an arrow. (C) Kymograph showing motility of mCherry-Rab5a on EEs (red) and motility of GFP_3Dyn (green). Dynein and the EE travel together until the dynein stops motility (filled arrowheads), whereas the EE continues retrograde motility (open arrowheads). The position relative to the tip is shown in the lower left corner. The location of the cell tip is indicated by an arrow. (D and E) Kymographs showing motility of mCherry-Rab5a on EEs (red) and motility of GFP_3Dyn (green). Dynein and the EEs travel together until dynein detaches from the organelles and moves without cargo (filled arrowheads). The EEs continue retrograde motility after a short pause (open arrowheads). The position relative to the tip is shown in the lower left corner. The location of the cell tip is indicated by an arrow. See also Movies S6–S8.

2011a, 2011b). The orientation of MT was investigated in strain AB33EB1Y and in strain AB5Dyn2^{ts}_ Peb1Y, which was generated by homologous integration of plasmid pPeb1Y_N (Lenz *et al.*, 2006) into the strains AB33 and AB5Dyn2^{ts}.

To visualize the MT minus ends, a 1013–base pair fragment near the 3′ end of the *grc1* gene (γ-tubulin ring complex 1; RefSeq accession number: XP_757621.1), followed by *egfp* and the *nos* terminator, the hygromycin resistance cassette, and 1061 base pairs of the downstream sequence were cloned into a cloning vector resulting in plasmid pGrc1G. The plasmid pGrc1G was digested with *Bsr*GI and two additional copies of *gfp* were introduced as *Bsr*GI fragments, resulting in the plasmid pGrc1-3G. The plasmid pGrc1-3G was digested with *Dra*I and integrated homologously into the *grc1* locus of strain AB33, resulting in AB33Grc1-3G. The plasmid potefGFP-Tub1 (Steinberg *et al.*, 2001) was digested with *Nco*I and *Nde*I to remove the *gfp* gene and replace it with *mCherry* gene, resulting in plasmid $po_mChTub1$. The plasmid popGRab5a (Schuster *et al.*, 2011b) was digested with *Bam*HI and *Bsr*GI to remove the *pagfp* gene and replace it with $pa_mCherry$ gene, resulting in the plasmid $popa_mChRab5a$.The plasmids $po_mChTub1$ and $popa_mChRab5a$ were digested with *Ssp*I and integrated at the succinate dehydrogenase locus of strain AB33Grc1-3G, resulting in AB33Grc1-3G_$_mChTub1 and AB33Grc1-3G_$pa_mChRab5a, respectively.

To analyze MT bundles, plasmid potefGFPTub1 (Steinberg *et al.*, 2001) was ectopically introduced into strain AB33, resulting in AB33GT. The strain AB33GT_Peb1R was obtained by homologous integration of plasmid pPeb1R_N (Lenz *et al.*, 2006) into AB33GT. The strain AB5Dyn2^{ts}_GT was generated by ectopic integration of plasmid potefGFPTub1 in the strain AB5Dyn2^{ts}. For colocalization studies of dynein and MT, plasmid potefGFPTub1 was ectopically integrated into strain $AB33G_3Dyn2$, resulting in $AB33G_3Dyn2\_GT$. For strain AB33_ΔKin3_r Dyn1_GRab5a, the phleomycin resistance cassette of plasmid pcrgDyn1 (Lenz *et al.*, 2006) was replaced by the hygromycin resistance cassette, resulting in plasmid pcrgDyn1-H. This plasmid was transformed in strain AB33_ΔKin3_GRab5a. potagRRab5a was generated by replacing the paGFP in plasmid popaGRab5a (Schuster *et al.*, 2011b) with TagRFP (Evrogen, Moscow, Russia). The resulting plasmid potagRRab5a was linearized with *Age*I for homologous integration at the succinate dehydrogenase locus of strain AB33ΔKin3_Kin3^{ts}G, resulting in AB33ΔKin3_ Kin3^{ts}G_tagRRab5a.

To visualize Kin3-GFP, a 1036–base pair fragment near the 3′ end of the gene, followed by *egfp* and the *nos* terminator, the hygromycin resistance cassette, and 1032 base pairs of the downstream sequence were cloned into a cloning vector, resulting in plasmid pKin3G_H. The plasmid was integrated into the native kin3 locus, resulting in strain AB33Kin3G. All strains and plasmids used in this study are summarized in Table 1.

Generation of a temperature-sensitive *kinesin-3* mutant

To generate the temperature-sensitive mutants in *kin3*, the error-prone PCR approach was used (modified from Spee *et al.* [1993]). The *kin3* gene was cloned behind its own promoter and followed by the terminator sequences into a self-replicating plasmid, resulting in plasmid pNEBUH-Kin3. Primers were designed to PCR-amplify four fragments that partially overlapped and covered the entire open reading frame (ORF) of *kin3*. Each primer pair was used in eight PCR reactions, each using only 10 or 20% of one of the four deoxyribonucleotide triphosphates. The products from these 32 PCR reactions were pooled and, together with the linearized plasmid pNEBUH-Kin3 that lacked the *kin3* ORF, were transformed into the yeast *S. cerevisiae* for in vivo recombination (further details are given in Schuster *et al.*, 2011b). The resulting plasmid pool was obtained from yeast and amplified in *Escherichia coli*. After recovery, the plasmid pool was transformed into strain AB33ΔKin3 according to published procedures (Schulz *et al.*, 1990). Transformed cells were replica-plated from transformation plates, where they can be grown as yeast-like cells without phenotype, onto hyphal growth-inducing nitrate-minimal (NM) plates, supplemented with 1% glucose (Brachmann *et al.*, 2001). After cells were incubated at 22 and 32°C for 3 d, restoration of hyphal growth at low temperature, but not at high temperature, was monitored. Fifteen positive colonies were collected; their self-replicating pNEBUH vectors carrying mutated *kin3^{ts}* genes were isolated and transformed into strain AB33ΔKin3_GRab5a. EE motility was analyzed in all strains at 22 and 32°C, and one strain was selected that showed normal motility at 22°C but almost no motility after 5 min at 32°C. This *kin3^{ts}* allele was ectopically integrated into strains $AB33\Delta Kin3\_G_3Dyn2$ and AB33ΔKin3_paGFP-Rab5a, resulting in $AB33\Delta Kin3\_Kin3^{ts}\_G_3Dyn2$ and AB33ΔKin3_Kin3^{ts}_paGFP-Rab5a, respectively. The plasmid pKin3^{ts}G was generated through in vivo recombination in the yeast *S. cerevisiae* by cloning a PCR-amplified fragment of *egfp-GFP-Tnos* (1016 base pairs) with 30–base pair overhang sequences into *Bsr*GI-digested plasmid pKin3^{ts}. The resulting plasmid pKin3^{ts}-G was digested

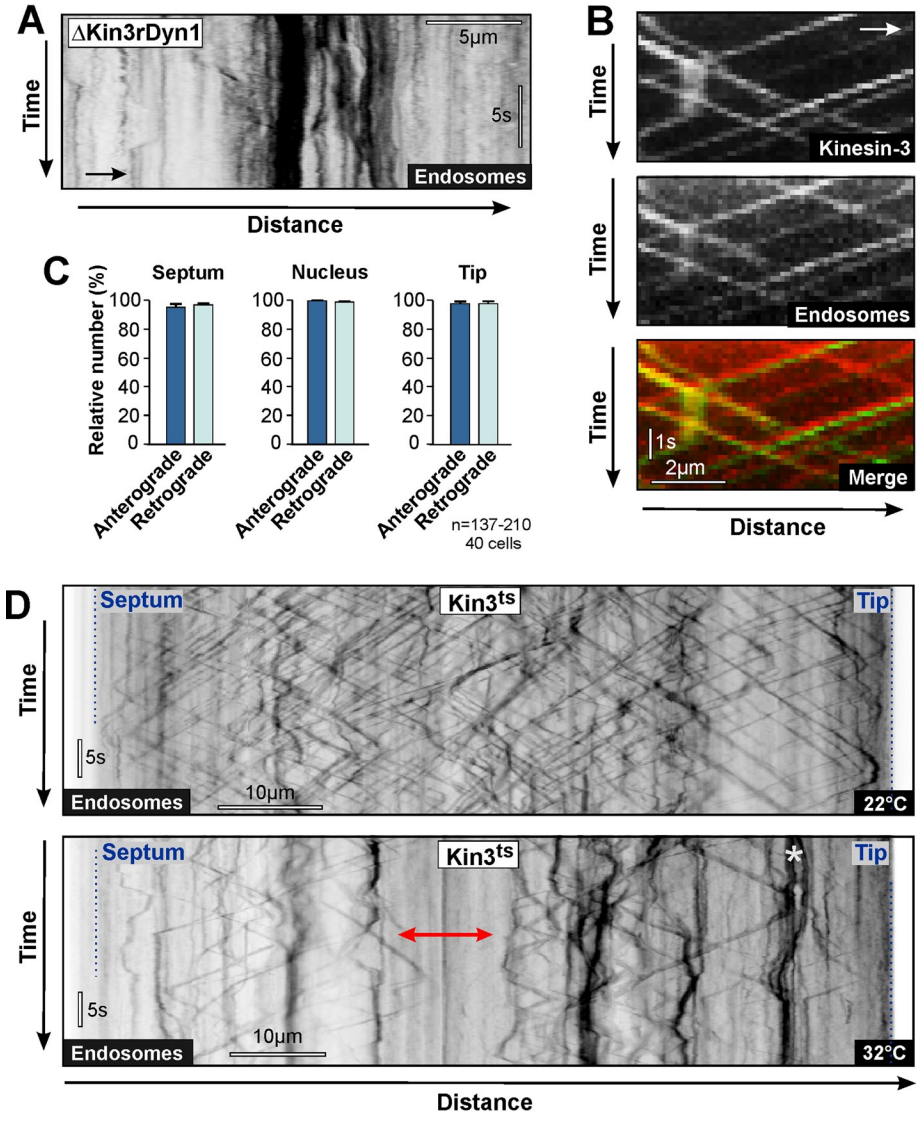

FIGURE 7: Run length of EEs in temperature-sensitive kinesin-3 mutants. (A) Kymograph showing immobile EE (GFP-Rab5a) in hyphal cells of a conditional dynein/Δkinesin-3 double mutant at restrictive conditions. The location of the cell tip is indicated by an arrow. See Movie S9. (B) Kymographs showing comigration of Kin3-GFP and EEs (labeled with mCherry-Rab5a). Kinesin-3 is bound to anterograde and retrograde organelles. Note that in the overlay both images were slightly shifted against each other to demonstrate colocalization of Kin3-GFP and mCherry-Rab5a on EEs. The location of the cell tip is indicated by an arrow. See also Movie S10 for Kin3-GFP moving in the retrograde direction. (C) Bar chart showing the relative numbers of Kin3-GFP that colocalize with mCherry-Rab5a labeled EEs. Anterograde: motility toward the hyphal tip; retrograde: motility toward the septum. Sample size (N) for EEs and total number of analyzed cells are given. (D) Kymographs showing motility of EEs in a Kin3^{ts} mutant at permissive (22°C) and restrictive (32°C) temperature. Note that at restrictive temperature EE clusters are formed (*) and EEs motility did not overcome the middle part of the cell (red arrow), thereby no longer connecting the apical and the rear cell regions. Cell ends are indicated by dotted lines.

with *Psi*I and *Hpa*I and transformed into AB33ΔKin3, resulting in AB33ΔKin3_Kin3^{ts}G.

Growth conditions

All cultures of *U. maydis*, with the exception of kinesin-3 and dynein temperature sensitive strains, were grown overnight at 28°C in complete medium (CM; Holliday, 1974) containing 1% (wt/vol) glucose, shaken at 200 rpm. Hyphal growth was induced by shifting to NM liquid medium supplemented with 1% (wt/vol) glucose (Brachmann *et al.*, 2001). The strains AB33ΔKin3_Kin3^{ts}_GRab5a, AB33ΔKin3_Kin3^{ts}_paGRab5a, AB33ΔKin3_Kin3^{ts}_G$_3$Dyn2, AB33ΔKin3_Kin3^{ts}G_tagRRab5a, AB5Dyn2^{ts}_GRab5a, and AB5Dyn2^{ts}_GT were grown for 10 h at 22°C in CM containing 1% (wt/vol) glucose, shaken at 200 rpm. Hyphal growth was induced overnight at 22°C, and cells were shifted to 32°C when required. Strain AB33ΔKin3_rDyn1_GRab5a was grown overnight in CM containing 1% (wt/vol) arabinose. Hyphal growth was induced by shifting to NM liquid medium supplemented with 1% arabinose for 8 h. For dynein depletion, cells were shifted to NM liquid medium supplemented with 1% glucose for 12–14 h.

Laser-based epifluorescence microscopy

Microscopy was essentially done as previously described (Schuster *et al.*, 2011a, 2011b). In brief, hyphal cells were placed on a 2% agar cushion and cargo or motor motility was observed using an IX81 motorized inverted microscope (Olympus, Hamburg, Germany) equipped with a VS-LMS4 Laser-Merge-System using solid-state lasers (488 nm/75mW and 561 nm/75 mW; Visitron Systems, Munich, Germany). Photoactivation and photobleaching experiments were done using a 2D-VisiFRAP system (Visitron Systems) consisting of a 405-nm/60-mW diode laser, which was dimmed by a neutral density 0.6 filter, resulting in 15-mW output power. Simultaneous observation of RFP and GFP fluorescence was done using a Dual-View microimager (Optical Insights, Tucson, AZ) and filter sets consisting of excitation dual-line beam splitter (z491/561; Chroma, Rockingham, VT), the emission beam splitter in the Dual-View (565 DCXR; Chroma), an ET-Bandpass 525/50 (Chroma), and a BrightLine HC 617/73 (Semrock, Rochester, NY). For temperature-dependent experiments, the objectives were cooled or heated using a metal hull connected to a water bath (Huber, Offenburg, Germany). Images were captured using a charge-coupled device camera (Photometrics CoolSNAP HQ2; Roper Scientific, Ottobrunn, Germany). All parts of the microscope system were under the control of the software package MetaMorph (Molecular Devices, Downingtown, PA).

Analysis of MT bundling and orientation

Hyphal cells of strain AB33Peb1Y were placed on 2% agar cushions and image sequences of 35 planes at an exposure time of 300 ms were taken. The direction of plus-end elongation was determined in kymographs generated in the program MetaMorph.

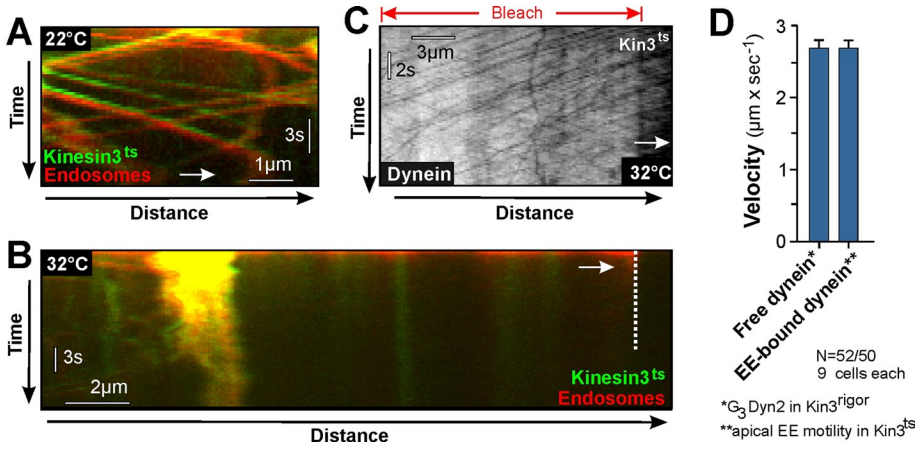

FIGURE 8: Motility of EEs, dynein and the temperature-sensitive kinesin-3^{ts} protein in kinesin-3 mutants. (A) Kymograph showing colocalization of the temperature-sensitive mutant motor protein kinesin-3^{ts}-GFP and mCherry-Rab5a at permissive temperature. The motor localizes to anterograde and retrograde EEs. Note that in the overlay both images were slightly shifted against each other to better demonstrate colocalization. The location of the cell tip is indicated by an arrow. (B) Kymograph showing colocalization of the temperature-sensitive mutant motor protein kinesin-3^{ts}-GFP and mCherry-Rab5a after 5 min at restrictive temperature. Kinesin-3^{ts}-GFP still localizes to the EEs, which have left the apical region of the hyphal cell due to the activity of dynein and form large aggregates at ~12 µm behind the cell tip. Note that this position corresponds with the transition from the unipolar to the antipolar region of the MT array. The location of the cell tip is indicated by an arrow. See also Movie S11. (C) Kymograph showing retrograde motility of GFP-labeled dynein in kinesin-3^{ts} cells at restrictive temperature. Cells were prebleached (indicated by red arrow and "Bleach") using a 405-nm laser to reduce the interference with dynein signals moving in the anterograde direction (Schuster *et al.*, 2011a, 2011b). (D) Bar chart showing the retrograde velocity of dynein motors that are not bound to their cargo ("free dynein," measured in a strain where EEs are immobilized [Schuster *et al.*, 2011b]) and velocity of retrograde EEs within the unipolar region of MT array in cells where kinesin-3 was inactivated ("EE-bound dynein"). No significant difference in velocity was found. Sample size (N) for free dynein signals or EEs moving in the retrograde directionand total number of analyzed cells are given.

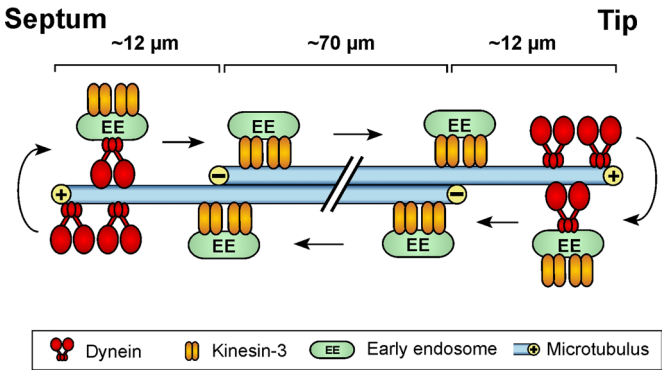

FIGURE 9: Model for motor cooperation in long-range retrograde EE motility. EEs arrive at MT plus ends and get loaded onto dynein that takes the organelles through the unipolar MT array toward minus ends. At this time, kinesin-3 is a passive cargo. Cytoplasmic MTOCs are absent from the regions near the cell end, and their appearance at ~12 µm behind the tip indicates the beginning of the antipolar MT array. This MT arrangement allows kinesin-3 to continue retrograde motility of the EEs until they reach the dynein accumulation at the plus ends near the septum. Note that EE trafficking is slightly asymmetric, with more motility found near the hyphal tip. In addition, the majority of the retrograde EEs reverse transport direction before reaching the septum due to stochastic binding and unbinding of the organelles to dynein (Schuster *et al.*, 2011a).

Error bars were calculated using the modified Wald method (Agresti and Coull, 1998).

Hyphal cells were fixed with 1% formaldehyde (PolyScience, Niles, IL) to avoid MT motility. Z-stacks were taken at 300-nm step size using a Piezo drive (Piezosystem Jena GmbH, Jena, Germany). Z-stacks of MTs were processed by 100 iterations of three-dimensional deconvolution. Maximum projections, cross-sections, and three-dimensional reconstructions of the resulting images were created using AutoQuantX software (AutoQuant Imaging, Troy, NY). Fluorescence-intensity measurements of the MT signals were carried out using MetaMorph. To determine the intensity of single MTs, the mean fluorescence intensity of the 10 faintest singles was determined. The degree of MT bundling was estimated by comparison to these signals.

Visualization of the behavior of EE at the MT minus ends

Photoactivation of EEs in strain AB33Grc--3G_ pa$_m$ChRab5a was done with a 150-ms light pulse using a 60-mW/405-nm laser at 4% output power. Dual-image series of 100 frames were taken with the 488-nm and 561-nm observation lasers at 30% output power and an exposure time of 150 ms and binning 2. The behavior of EEs at the MT minus ends were analyzed in overlays of kymographs generated in MetaMorph from these image series.

Visualization and analysis of the run length of fluorescent motor proteins and EEs

Motors were visualized in hyphal cells of strains AB33Kin3G, AB-33G$_3$Dyn2, and AB33ΔKin3_Kin3^{ts}_G$_3$Dyn2. To visualize retrograde motility of motors, two different sets of image series were acquired. The extended runs were investigated by photobleaching the whole cell (excluding the apical 10 µm) with a 405-nm laser at 100% output power at 150-ms exposure and beam diameter of 30 pixels using the UPlanSApo 60×/1.35 oil objective. After a pause for 10 s, streams of 400 planes were taken using a 488-nm observation laser at 40% output power and an exposure time of 250 ms, a 250-ms interval between frames, and image binning 2. For short runs, a second set of image series was acquired using a PlanApo 100×/1.45 oil total internal reflection fluorescence objective. In this case, only 30–40 µm of the hyphal cell (excluding the apical 3–5 µm) was photobleached. This was followed by immediate observation using the 488-nm observation laser at 100% output power and 50-ms exposure time. For each strain, the "long" and the "short" set was comprised of 20 movies and the run lengths were analyzed in kymographs were generated in MetaMorph from these image series.

For analysis of the temperature-sensitive strains AB33ΔKin3_Kin3^{ts}_G$_3$Dyn2 and AB33ΔKin3_Kin3^{ts}_paGRab5a, the objective and the agar pads were precooled to 22°C or preheated to 32 °C before the hyphal cells were observed. Inactivation of Kin3^{ts} was done by preincubating the culture at 32°C for 5 min (for AB33ΔKin3_Kin3^{ts}_G$_3$Dyn2) or by keeping cells on the prewarmed

Strain/plasmid	Genotype	Source
AB33nRFP	*a2* P*narbW2* P*narbE1*, *ble*^{R}/poNLS3RFP	Schuster *et al.*, 2011a
AB33Peb1Y	*a2* P*narbW2* P*narbE1*, P*peb1-peb1-yfp*, *ble*^{R,} *nat*^{R}	This study
AB33Grc1-3G	*a2* P*narbW2* P*narbE1*, P*grc1-grc1-3gfp*, *ble*^{R}, *hyg*^{R}	This study
AB33Grc1-3G_ChT	*a2* P*narbW2* P*narbE1*, P*grc1-grc1-3gfp*, *ble*^{R}, *hyg*^{R}/po$_m$ChTub1	This study
AB33GT	*a2* P*narbW2* P*narbE1*, *ble*^{R}/potefGFPTub1	This study
AB33GT_Peb1R	*a2* P*narbW2* P*narbE1*, P*peb1-peb1-rfp*, *ble*^{R}, *nat*^{R}/potefGFPTub1	Schuchardt *et al.*, 2005
AB33paGRab5a	*a2* P*narbW2* P*narbE1*, *ble*^{R}/popaGRab5a	Schuster *et al.*, 2011a
AB33Grc1-3G_ paChRab5a	*a2* P*narbW2* P*narbE1*, P*grc1-3gfp*, *ble*^{R}, *hyg*^{R}/popa$_m$ChRab5a	This study
AB33Ch$_3$Dyn2_GT	*a2* P*narbW2* P*narbE1*, P*dyn2-3xmCherry-dyn2*, *ble*^{R}, *hyg*^{R}/ potefGFPTub1	This study
AB33G$_3$Dyn2	*a2* P*narbW2* P*narbE1*, P*dyn2-3xegfp-dyn2*, *ble*^{R}, *hyg*^{R}	Lenz *et al.*, 2006
AB33G$_3$Dyn2_ChRab5a	*a2* P*narbW2* P*narbE1*, P*dyn2-3xegfp-dyn2*, *ble*^{R}, *hyg*^{R}/ po$_m$ChRab5a	Schuster *et al.*, 2011a
AB5Dyn2^{ts}_GRab5a	*a1*P*narbW2* P*narbE1*, P*dyn2-dyn2*^{ts}, *ble*^{R}, *hyg*^{R}/poGRab5a	This study
AB5Dyn2^{ts}_GT	*a1*P*narbW2* P*narbE1*, P*dyn2-dyn2*^{ts}, *ble*^{R}, *hyg*^{R}/potefGFPTub1	This study
AB5Dyn2^{ts}_ Peb1Y	*a1*P*narbW2* P*narbE1*, P*dyn2-dyn2*^{ts}, P*peb1-peb1-yfp ble*^{R}, *hyg*^{R}, *nat*^{R}	This study
AB33Kin3G	*a2* P*narbW2* P*narbE1*, P*kin3-kin3-egfp*, *ble*^{R}, *hyg*^{R}	This study
AB33ΔKin3_Rab5a	*a2* P*narbW2* P*narbE1*, Δ*kin3*, *ble*^{R}, *nat*^{R}/poGRab5a	This study
AB33ΔKin3_rDyn1_GRab5a	*a2* P*narbW2* P*narbE1*, Δ*kin3*, P*crg-dyn1*, *ble*^{R}, *nat*^{R}, *hyg* ^{R}/ poGRab5a	This study
AB33ΔKin3_Kin3G_ChRab5a	*a2* P*narbW2* P*narbE1*, Δ*kin3*, *ble*^{R}, *hyg*^{R}/pKin3G/po$_m$ChRab5a	This study
AB33ΔKin3_Kin3^{ts}_GRab5a	*a2* P*narbW2* P*narbE1*, Δ*kin3*, *ble*^{R}, *nat*^{R},/pKin3^{ts}/poGRab5a	This study
AB33ΔKin3_Kin3^{ts}_paGRab5a	*a2* P*narbW2* P*narbE1*, Δ*kin3*, *ble*^{R}, *nat*^{R},/pKin3^{ts}/popaGRab5a	This study
AB33ΔKin3_Kin3^{ts}G_tagRRab5a	*a2* P*narbW2* P*narbE1*, Δ*kin3*, *ble*^{R}, *nat*^{R},/ pKin3^{ts}G/potagRRab5a	This study
AB33ΔKin3_G$_3$Dyn2_Kin3^{ts}	*a2* P*narbW2* P*narbE1*, Δ*kin3*, P*dyn2-3xegfp-dyn2*, *ble*^{R}, *nat*^{R}, *cbx*^{R} /pKin3^{ts}	This study
poNLS3RFP	P*otef-gal4s-mrfp-mrfp-mrfp*, *nat*^{R}	Schuster *et al.*, 2011a
po$_m$ChTub1	P*otef-mCherry-tub1 cbx*^{R}	This study
potefGFPTub1	P*otef-egfp-tub1*, *cbx*^{R}	Steinberg *et al.*, 2001
popaGRab5a	P*otef-pagfp-rab5a*, *cbx*^{R}	Schuster *et al.*, 2011b
popa$_m$ChRab5a	P*otef-pamcherry-rab5a*, *cbx*^{R}	This study
po$_m$ChRab5a	P*otef-mcherry-rab5a*, *nat*^{R}	Schuster *et al.*, 2011a
poGRab5a	P*otef-egfp-rab5a*, *nat*^{R}	Schuster *et al.*, 2011b
pKin3G	P*kin3-kin3-gfp*, *cbx*^{R}	Wedlich-Söldner *et al.*, 2002a
pKin3^{ts}	P*kin3-kin3*^{ts}, *hyg*^{R}	This study
pKin3^{ts}G	P*kin3-kin3*^{ts}*-gfp*, *hyg*^{R}	This study
potagRRab5a	P*otef-tagrfp-rab5a*, *cbx*^{R}	This study

a, *b*, mating type loci; P, promoter; -, fusion; *hyg*^{R}, hygromycin resistance; *ble*^{R}, phleomycin resistance; *nat*^{R}, nourseothricin resistance; *cbx*^{R}, carboxin resistance; ^{ts}, temperature-sensitive allele; Δ, deletion; /, ectopically integrated; *crg*, conditional arabinose-induced promoter; *otef*, constitutive promoter; *nar*, conditional nitrate reductase promoter; *E1*, *W2*, genes of the *b* mating-type locus; *egfp*, enhanced green fluorescent protein; *pagfp:* photoactivatable monomeric green fluorescent protein; *mrfp*, *tagrfp*, monomeric red fluorescent protein; *mCherry*, monomeric Cherry; *yfp*, yellow fluorescent protein; NLS, nuclear localization signal of the GAL-4 DNA-binding domain from pC-ACT1 (Clontech, Mountain View, CA); GT, gfp-tubulin; *peb1*, EB1-like plus end–binding protein; *dyn2*: C-terminal half of the dynein heavy chain; *dyn1*: N-terminal half of the dynein heavy chain; *rab5a*, small endosomal Rab5-like GTPase; *kin3*, kinesin-3; *grc1*: γ-tubulin ring complex protein 1.

TABLE 1: Strains and plasmids used in this study.

microscope stage for ~3 min before the image series was taken. Dynein motility in AB33ΔKin3_Kin3^{ts}_G$_3$Dyn2 was recorded as described above, whereas EE motility in AB33ΔKin3_Kin3^{ts}_GRab5a was observed at 15% output power of the 488-nm laser and 150-ms exposure time and binning 1. Photoactivation of EEs in strains AB33paGRab5a and AB33ΔKin3_Kin3^{ts}_paGRab5a was done with a 100-ms light pulse using a 60-mW/405-nm laser at 2% output power. An image series of 600 frames was taken with the 488-nm observation laser at 15% output power, an exposure time of 100 ms, image interval of 300 ms, and image binning 2. Run

lengths were analyzed in kymographs generated in MetaMorph from these image series.

Analysis of the colocalization of EE with dynein and kinesin-3

To analyze the degree of colocalization of kinesin-3 and EE in strain AB33ΔKin3_Kin3G_ChRab5a, a region of 10 μm in length at 5 μm behind the tip or septum or around the nucleus was irradiated by using 100% output power of 405-nm laser for 75 ms with a beam diameter of 30 pixels. This was followed by immediate observation using the Dual-View microimager and the 488-nm observation laser at 100% output power and the 561-nm observation laser at 25% output power at an exposure time of 200 ms and image binning 1. Kymographs from both fluorescence channels were overlaid and colocalization was analyzed. For the colocalization of dynein and EEs, 50 μm of the hyphal cell, beginning 5 μm behind the tip, was photobleached with the 405-nm laser at 100% output power for 150 ms with a beam diameter of 30 pixels. Subsequently, 100 frame movies were taken without delay or after 10 or 15 s using the 488-nm observation laser at 70% output power and the 561 laser at 30% output power and an exposure time of 150 ms. Again, kymographs were merged and the degree of colocalization was analyzed in these overlaid images.

ACKNOWLEDGMENTS

This work was supported by a grant from the Biotechnology and Biological Sciences Research Council (BB/F022956/1). The Max Planck Institute for Terrestrial Microbiology in Marburg is acknowledged for providing equipment. We thank M. Feldbrügge for providing strain AB5Dyn2^{ts}, which was used to generate AB33G$_3$Dyn2_ChRab5a and AB5Dyn2^{ts}_GT. I. Schuchardt is gratefully acknowledged for generating strain AB33Peb1Y, and P. Ashwin and C. Lin are gratefully acknowledged for their help with statistical analysis. We thank several lab members for discussion.

REFERENCES

Adamikova L, Straube A, Schulz I, Steinberg G (2004). Calcium signaling is involved in dynein-dependent microtubule organization. Mol Biol Cell 15, 1969–1980.

Agresti A, Coull BA (1998). Approximate is better than "exact" for interval estimation of binomial proportions. Am Statistician 52, 119–126.

Ally S, Larson AG, Barlan K, Rice SE, Gelfand VI (2009). Opposite-polarity motors activate one another to trigger cargo transport in live cells. J Cell Biol 187, 1071–1082.

Baas PW (1999). Microtubules and neuronal polarity: lessons from mitosis. Neuron 22, 23–31.

Baas PW, Deitch JS, Black MM, Banker GA (1988). Polarity orientation of microtubules in hippocampal neurons: uniformity in the axon and nonuniformity in the dendrite. Proc Natl Acad Sci USA 85, 8335–8339.

Baas PW, Lin S (2010). Hooks and comets: The story of microtubule polarity orientation in the neuron. Dev Neurobiol 71, 403–418.

Baas PW, Slaughter T, Brown A, Black MM (1991). Microtubule dynamics in axons and dendrites. J Neurosci Res 30, 134–153.

Barkus RV, Klyachko O, Horiuchi D, Dickson BJ, Saxton WM (2008). Identification of an axonal kinesin-3 motor for fast anterograde vesicle transport that facilitates retrograde transport of neuropeptides. Mol Biol Cell 19, 274–283.

Black MM, Baas PW (1989). The basis of polarity in neurons. Trends Neurosci 12, 211–214.

Blake-Hodek KA, Cassimeris L, Huffaker TC (2010). Regulation of microtubule dynamics by Bim1 and Bik1, the budding yeast members of the EB1 and CLIP-170 families of plus-end tracking proteins. Mol Biol Cell 21, 2013–2023.

Bottin A, Kämper J, Kahmann R (1996). Isolation of a carbon source-regulated gene from *Ustilago maydis*. Mol Gen Genet 253, 342–352.

Brachmann A, Weinzierl G, Kämper J, Kahmann R (2001). Identification of genes in the bW/bE regulatory cascade in *Ustilago maydis*. Mol Microbiol 42, 1047–1063.

Burton PR, Paige JL (1981). Polarity of axoplasmic microtubules in the olfactory nerve of the frog. Proc Natl Acad Sci USA 78, 3269–3273.

Chevalier-Larsen E, Holzbaur EL (2006). Axonal transport and neurodegenerative disease. Biochim Biophys Acta 1762, 1094–1108.

Deacon SW, Nascimento A, Serpinskaya AS, Gelfand VI (2005). Regulation of bidirectional melanosome transport by organelle bound MAP kinase. Curr Biol 15, 459–463.

Deacon SW, Serpinskaya AS, Vaughan PS, Lopez Fanarraga M, Vernos I, Vaughan KT, Gelfand VI (2003). Dynactin is required for bidirectional organelle transport. J Cell Biol 160, 297–301.

Delcroix JD, Valletta JS, Wu C, Hunt SJ, Kowal AS, Mobley WC (2003). NGF signaling in sensory neurons: evidence that early endosomes carry NGF retrograde signals. Neuron 39, 69–84.

Duncan JE, Goldstein LS (2006). The genetics of axonal transport and axonal transport disorders. PLoS Genetics 2, e124.

Gross SP (2004). Hither and yon: a review of bi-directional microtubule-based transport. Phys Biol 1, R1–R11.

Gross SP, Tuma MC, Deacon SW, Serpinskaya AS, Reilein AR, Gelfand VI (2002a). Interactions and regulation of molecular motors in *Xenopus* melanophores. J Cell Biol 156, 855–865.

Gross SP, Welte MA, Block SM, Wieschaus EF (2002b). Coordination of opposite-polarity microtubule motors. J Cell Biol 156, 715–724.

Guillaud L, Wong R, Hirokawa N (2008). Disruption of KIF17-Mint1 interaction by CaMKII-dependent phosphorylation: a molecular model of kinesin-cargo release. Nat Cell Biol 10, 19–29.

Ha J, Lo KW, Myers KR, Carr TM, Humsi MK, Rasoul BA, Segal RA, Pfister KK (2008). A neuron-specific cytoplasmic dynein isoform preferentially transports TrkB signaling endosomes. J Cell Biol 181, 1027–1039.

Heidemann SR, Landers JM, Hamborg MA (1981). Polarity orientation of axonal microtubules. J Cell Biol 91, 661–665.

Hendricks AG, Perlson E, Ross JL, Schroeder HW 3rd, Tokito M, Holzbaur EL (2010). Motor coordination via a tug-of-war mechanism drives bidirectional vesicle transport. Curr Biol 20, 697–702.

Hirokawa N, Sato-Yoshitake R, Yoshida T, Kawashima T (1990). Brain dynein (MAP1C) localizes on both anterogradely and retrogradely transported membranous organelles in vivo. J Cell Biol 111, 1027–1037.

Hirokawa N, Takemura R (2004). Molecular motors in neuronal development, intracellular transport and diseases. Curr Opin Neurobiol 14, 564–573.

Holliday R (1974). *Ustilago maydis*. In Handbook of Genetics, ed. RC King, New York: Plenum Press, 1, 575–595.

Howard J, Hudspeth AJ, Vale RD (1989). Movement of microtubules by single kinesin molecules. Nature 342, 154–158.

Howard RJ (1981). Ultrastructural analysis of hyphal tip cell growth in fungi: Spitzenkörper, cytoskeleton and endomembranes after freeze-substitution. J Cell Sci 48, 89–103.

Howard RJ, Aist JR (1979). Hyphal tip cell ultrastructure of the fungus *Fusarium*: improved preservation by freeze-substitution. J Ultrastruc Res 66, 224–234.

Howe CL, Mobley WC (2005). Long-distance retrograde neurotrophic signaling. Curr Opin Neurobiol 15, 40–48.

Kapitein LC, Schlager MA, Kuijpers M, Wulf PS, van Spronsen M, MacKintosh FC, Hoogenraad CC (2010). Mixed microtubules steer dynein-driven cargo transport into dendrites. Curr Biol 20, 290–299.

King SJ, Schroer TA (2000). Dynactin increases the processivity of the cytoplasmic dynein motor. Nat Cell Biol 2, 20–24.

Klumpp S, Lipowsky R (2005). Cooperative cargo transport by several molecular motors. Proc Natl Acad Sci USA 102, 17284–17289.

Koonce MP, Schliwa M (1986). Reactivation of organelle movements along the cytoskeletal framework of a giant freshwater ameba. J Cell Biol 103, 605–612.

Koushika SP, Schaefer AM, Vincent R, Willis JH, Bowerman B, Nonet ML (2004). Mutations in *Caenorhabditis elegans* cytoplasmic dynein components reveal specificity of neuronal retrograde cargo. J Neurosci 24, 3907–3916.

Larsen KS, Xu J, Cermelli S, Shu Z, Gross SP (2008). BicaudalD actively regulates microtubule motor activity in lipid droplet transport. PloS One 3, e3763.

Lee JR, Shin H, Ko J, Choi J, Lee H, Kim E (2003). Characterization of the movement of the kinesin motor KIF1A in living cultured neurons. J Biol Chem 278, 2624–2629.

Lenz JH, Schuchardt I, Straube A, Steinberg G (2006). A dynein loading zone for retrograde endosome motility at microtubule plus-ends. EMBO J 25, 2275–2286.

Ligon LA, Tokito M, Finklestein JM, Grossman FE, Holzbaur EL (2004). A direct interaction between cytoplasmic dynein and kinesin I may coordinate motor activity. J Biol Chem 279, 19201–19208.
Mallik R, Petrov D, Lex SA, King SJ, Gross SP (2005). Building complexity: an in vitro study of cytoplasmic dynein with in vivo implications. Curr Biol 15, 2075–2085.
Miaczynska M, Pelkmans L, Zerial M (2004). Not just a sink: endosomes in control of signal transduction. Curr Opin Cell Biol 16, 400–406.
Miller KE, DeProto J, Kaufmann N, Patel BN, Duckworth A, Van Vactor D (2005). Direct observation demonstrates that Liprin-α is required for trafficking of synaptic vesicles. Curr Biol 15, 684–689.
Müller MJ, Klumpp S, Lipowsky R (2008). Tug-of-war as a cooperative mechanism for bidirectional cargo transport by molecular motors. Proc Natl Acad Sci USA 105, 4609–4614.
Nogales E, Whittaker M, Milligan RA, Downing KH (1999). High-resolution model of the microtubule. Cell 96, 79–88.
Pedersen LB, Geimer S, Rosenbaum JL (2006). Dissecting the molecular mechanisms of intraflagellar transport in *Chlamydomonas*. Curr Biol 16, 450–459.
Reck-Peterson SL, Yildiz A, Carter AP, Gennerich A, Zhang N, Vale RD (2006). Single-molecule analysis of dynein processivity and stepping behavior. Cell 126, 335–348.
Rogers SL, Tint IS, Fanapour PC, Gelfand VI (1997). Regulated bidirectional motility of melanophore pigment granules along microtubules in vitro. Proc Natl Acad Sci USA 94, 3720–3725.
Schuchardt I, Assmann D, Thines E, Schuberth C, Steinberg G (2005). Myosin-V, Kinesin-1, and Kinesin-3 cooperate in hyphal growth of the fungus *Ustilago maydis*. Mol Biol Cell 16, 5191–5201.
Schulz B, Banuett F, Dahl M, Schlesinger R, Schafer W, Martin T, Herskowitz I, Kahmann R (1990). The *b* alleles of *U. maydis*, whose combinations program pathogenic development, code for polypeptides containing a homeodomain-related motif. Cell 60, 295–306.
Schuster M, Assmann MA, Lenz P, Lipowsky R, Steinberg G (2011a). Transient binding of dynein controls bidirectional long-range motility of early endosomes. Proc Natl Acad Sci USA 108, 3618–3623.
Schuster M, Kilaru S, Ashwin P, Congping L, Severs NJ, Steinberg G (2011b). Controlled and stochastic retention concentrates dynein at microtubule ends to keep endosomes on track. EMBO J 30, 652–664.
Shubeita GT, Tran SL, Xu J, Vershinin M, Cermelli S, Cotton SL, Welte MA, Gross SP (2008). Consequences of motor copy number on the intracellular transport of kinesin-1-driven lipid droplets. Cell 135, 1098–1107.
Smith GA, Pomeranz L, Gross SP, Enquist LW (2004). Local modulation of plus-end transport targets herpesvirus entry and egress in sensory axons. Proc Natl Acad Sci USA 101, 16034–16039.
Soppina V, Rai AK, Ramaiya AJ, Barak P, Mallik R (2009). Tug-of-war between dissimilar teams of microtubule motors regulates transport and fission of endosomes. Proc Natl Acad Sci USA 106, 19381–19386.
Spee JH, de Vos WM, Kuipers OP (1993). Efficient random mutagenesis method with adjustable mutation frequency by use of PCR and dITP. Nucleic Acids Res 21, 777–778.
Steinberg G (2007). On the move: endosomes in fungal growth and pathogenicity. Nat Rev Microbiol 5, 309–316.
Steinberg G, Perez-Martin J (2008). *Ustilago maydis*, a new fungal model system for cell biology. Trends Cell Biol 18, 61–67.
Steinberg G, Schliwa M, Lehmler C, Bölker M, Kahmann R, McIntosh JR (1998). Kinesin from the plant pathogenic fungus *Ustilago maydis* is involved in vacuole formation and cytoplasmic migration. J Cell Sci 111, 2235–2246.
Steinberg G, Schuster M (2011). The dynamic fungal cell. Fungal Biol Rev 25, 14–37.
Steinberg G, Wedlich-Söldner R, Brill M, Schulz I (2001). Microtubules in the fungal pathogen *Ustilago maydis* are highly dynamic and determine cell polarity. J Cell Sci 114, 609–622.
Straube A, Brill M, Oakley BR, Horio T, Steinberg G (2003). Microtubule organization requires cell cycle-dependent nucleation at dispersed cytoplasmic sites: polar and perinuclear microtubule organizing centers in the plant pathogen *Ustilago maydis*. Mol Biol Cell 14, 642–657.
Straube A, Hause G, Fink G, Steinberg G (2006). Conventional kinesin mediates microtubule-microtubule interactions in vivo. Mol Biol Cell 17, 907–916.
Subach FV, Patterson GH, Manley S, Gillette JM, Lippincott-Schwartz J, Verkhusha VV (2009). Photoactivatable mCherry for high-resolution two-color fluorescence microscopy. Nat Methods 6, 153–159.
Thorn KS, Ubersax JA, Vale RD (2000). Engineering the processive run length of the kinesin motor. J Cell Biol 151, 1093–1100.
Vale RD (2003). The molecular motor toolbox for intracellular transport. Cell 112, 467–480.
Vershinin M, Carter BC, Razafsky DS, King SJ, Gross SP (2007). Multiple-motor based transport and its regulation by Tau. Proc Natl Acad Sci USA 104, 87–92.
Wang Z, Khan S, Sheetz MP (1995). Single cytoplasmic dynein molecule movements: characterization and comparison with kinesin. Biophys J 69, 2011–2023.
Wedlich-Söldner R, Bölker M, Kahmann R, Steinberg G (2000). A putative endosomal t-SNARE links exo- and endocytosis in the phytopathogenic fungus *Ustilago maydis*. EMBO J 19, 1974–1986.
Wedlich-Söldner R, Schulz I, Straube A, Steinberg G (2002a). Dynein supports motility of endoplasmic reticulum in the fungus *Ustilago maydis*. Mol Biol Cell 13, 965–977.
Wedlich-Söldner R, Straube A, Friedrich MW, Steinberg G (2002b). A balance of KIF1A-like kinesin and dynein organizes early endosomes in the fungus *Ustilago maydis*. EMBO J 21, 2946–2957.
Welte MA (2004). Bidirectional transport along microtubules. Curr Biol 14, R525–R537.
Welte MA, Cermelli S, Griner J, Viera A, Guo Y, Kim DH, Gindhart JG, Gross SP (2005). Regulation of lipid-droplet transport by the perilipin homolog LSD2. Curr Biol 15, 1266–1275.
Welte MA, Gross SP, Postner M, Block SM, Wieschaus EF (1998). Developmental regulation of vesicle transport in *Drosophila* embryos, forces and kinetics. Cell 92, 547–557.
Zheng Y, Wildonger J, Ye B, Zhang Y, Kita A, Younger SH, Zimmerman S, Jan LY, Jan YN (2008). Dynein is required for polarized dendritic transport and uniform microtubule orientation in axons. Nat Cell Biol 10, 1172–1180.
Zhou HM, Brust-Mascher I, Scholey JM (2001). Direct visualization of the movement of the monomeric axonal transport motor UNC-104 along neuronal processes in living *Caenorhabditis elegans*. J Neurosci 21, 3749–3755.